

PAPER • OPEN ACCESS

Thermoelastic pulsed laser ablation of silver thin films with organic metal–SiO₂ adhesion layer in water: application to the sustainable regeneration of glass microfluidic reactors for silver nanoparticles

To cite this article: Tahir *et al* 2022 *J. Phys. Commun.* **6** 055005

View the [article online](#) for updates and enhancements.

You may also like

- [Effects of niobium pentoxide nanoparticles on the tribological properties of electrodeposited ZnNi coatings](#)
Hema C. R. Moreira, Jorge A. B. Oliveira, Neftali L. V. Carreño et al.
- [Reconstruction from Radon projections and orthogonal expansion on a ball](#)
Yuan Xu
- [Automatic classification of prostate stromal tissue in histological images using Haralick descriptors and Local Binary Patterns](#)
D L L Oliveira, M Z Nascimento, L A Neves et al.



PAPER

OPEN ACCESS



RECEIVED
16 March 2022REVISED
21 April 2022ACCEPTED FOR PUBLICATION
26 April 2022PUBLISHED
9 May 2022

Original content from this work may be used under the terms of the [Creative Commons Attribution 4.0 licence](#).

Any further distribution of this work must maintain attribution to the author(s) and the title of the work, journal citation and DOI.



Thermoelastic pulsed laser ablation of silver thin films with organic metal–SiO₂ adhesion layer in water: application to the sustainable regeneration of glass microfluidic reactors for silver nanoparticles

Tahir¹, Omar Ginoble Pandoli^{2,3} , Quaid Zaman^{1,4}, Guilherme C Concas¹, Mariana Gisbert¹, Marco Cremona¹, Fernando Lazaro Freire Jr¹, Isabel C S Carvalho¹, Pedro H C Bevilaqua², Druval Santos de Sá², Alexandre Pinto Canellas⁵, Vinicius Mattoso⁵ and Tommaso Del Rosso¹ 

¹ Department of Physics, Pontifícia Universidade Católica do Rio de Janeiro, Rua Marques de São Vicente, 22451-900, Rio de Janeiro, Brazil

² Department of Chemistry, Pontifícia Universidade Católica do Rio de Janeiro, Rua Marques de São Vicente, 22451-900, Rio de Janeiro, Brazil

³ Dipartimento di Farmacia, Università degli studi di Genova, Viale Benedetto XV, 7, 16132 Genova, Italy

⁴ Department of Physics, University of Buner, Buner, 17290, Pakistan

⁵ Department of Mechanical Engineering, Pontifícia Universidade Católica do Rio de Janeiro, Rua Marques de São Vicente, 22451-900, Rio de Janeiro, Brazil

E-mail: tommaso@puc-rio.br

Keywords: pulsed laser ablation in water, green cleaning method, metal thin films and nanomaterials, glass microfluidic reactors

Abstract

The synthesis of metal nanoparticles (NPs) using microfluidic reactors has become a major method for limiting reagent consumption and achieve a precise control of the morphological properties. Failure in realizing the reproducibility of the results is mostly associated with the accumulation of metallic nanostructures on the walls of the microfluidic devices, periodically removed by acid treatment. In this study, we show that ns-pulsed laser ablation (PLA) in water can be a safe, effective, and green method for the regeneration of clogged microfluidic reactors. The effect of the laser-pulse fluence on the removal of metallic nanostructures was studied for the first time on silver (Ag) thin films with a thickness of 50 nm deposited over SiO₂ substrates, using 3-mercaptopropyl trimethoxysilane as a chemical adhesion layer. As point of novelty, the experimental results show that at low fluence ($F < 0.1 \text{ J cm}^{-2}$), ablation is principally caused by delamination of the thin film associated with the thermoelastic force while thermal processes inducing phase conversion of the metal dominate at higher fluence. Low-fluence regimes are better suited for the single-pulse removal of the nanomaterial, whereas in high F regimes, we observed melting and recondensation of the metal on the SiO₂ surface so that multiple pulse interactions were necessary for complete ablation of the thin film. For the delamination and the phase transformation processes, the threshold fluences were 3.7×10^{-2} and $7.0 \times 10^{-2} \text{ J cm}^{-2}$, respectively. The experimental setup in the thermoelastic PLA regime was applied to unclog glass microfluidic devices used for synthesizing citrate-stabilized AgNPs. Using this simple and easily achievable laser-scanning experimental configuration, we demonstrated that PLA in water is a reliable and efficient technique, with results comparable to acidic treatment in terms of efficiency and time necessary for the complete removal of the Ag nanomaterial.

1. Introduction

Microreactor technology (MRT) is already a well-established technique for two main applications: (i) organic and inorganic synthesis in continuous-flow regimes [1]; and (ii) fabrication of analytical and medical sensor devices [2]. The materials used for the microfabrication of these chemical platform-tools, known as ‘lab-on-chip’ (LOC) [3] or ‘point-of-care’ (POC) [4], such as steel, glass, thermoplastic (a chip-like polymer), and paper, can be expensive. Depending on the specific application of the device, the right material, with the option to reuse it after cleaning the microchannels, should be chosen. Nowadays, considering the widespread use of glass-based

microfluidic devices, a sustainable, low-cost, and feasible methodology to clean and reuse them for repetitive experiments should be established [5]. The synthesis of metallic nanoparticles (NPs) using microfluidic devices has attracted great attention as it is a greener and more reproducible method than the sol-gel method synthesis [6]. Despite these advantages, the reduced volume of the microreactors can be attributed to intrinsically more vulnerable to a possible obstruction. The clogging of microchannels is attributed in literature to different mechanisms, such as sieving, bridging, and aggregation of the nano/micro particles. The mechanisms depend on the surface chemistry of the NPs, interparticle interactions, and the interactions of particles with the walls constituting the microdevice [7, 8]. To minimize or prevent clogging, different strategies have been proposed [9–11], including double-phase droplet-based microreactors [10, 12], segmented flow systems [13], coaxial flow systems [14, 15], and hydrodynamic flow focusing [16]. In any case, clogging of the microfluidic devices remains a critical issue in the field and they are cleaned by injecting solvents and, in case of failure, acid or base solutions depending on the specific materials that are clogged inside the microchannels. In this case, the system should be extensively rinsed with water after successful cleaning. In the context of a sustainable technology, the scientific community has been investigating methods to eliminate the use of acid solutions in experimental protocols dedicated to chemical synthesis, purification, or cleaning processes [17–21].

A physical process commonly used for removing materials from surfaces is laser ablation. This is a process of light-matter interaction where the material is removed from the surface of a target utilizing focused lasers [22]. It has several applications in modern technology, including precise micromachining of materials [23], dentistry applications [24], surgery [25, 26], conservation of cultural assets [27], and the production of different nanostructures and thin films [28, 29]. Noteworthy, there is strong interest and widespread activity reported in literature on the fabrication via pulsed laser ablation (PLA) of microfluidic devices with different geometries and different materials, principally glass, and poly(methyl methacrylate) (PMMA) or poly(dimethylsiloxane) (PDMS) [30–37]; however, to the best of our knowledge, there is no research currently in progress on the use of PLA for the regeneration of microfluidic reactors.

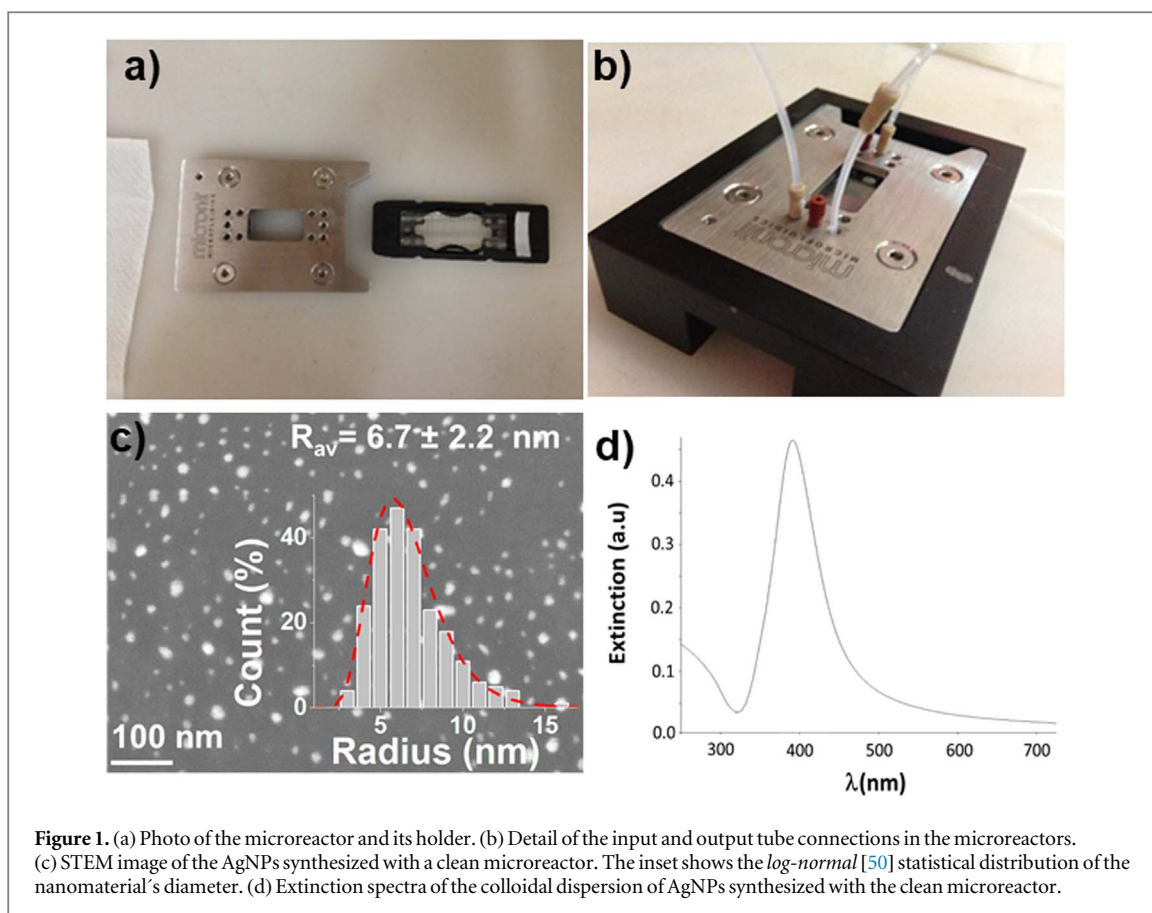
PLA can be performed using various types of pulsed laser sources, depending on the temporal length of the pulses (fs, ps, and ns). In the latter case, the PLA process is based on the absorption of the energy of the short laser pulse by the electrons of the surface of the targets, followed by phonon thermalization in times of the orders of ps. The mechanism related to the ejection of the material strongly depends on the temporal length of the laser pulses and the nature of the external environment [28]. Furthermore, the depth over which the incoming laser pulse is absorbed and the amount of material removed by a single-laser pulse depend on the environmental factors [38] along with the material's optical properties and the experimental laser-pulse parameters, such as wavelength, energy, and temporal length [28, 39–42].

In literature, investigation of the ablation of thin metal films is mostly performed under air environment for the precise micropatterning of electronic and optoelectronic devices, with ns-, ps-, or fs-laser pulses [43–46]. Laser writing with fs-laser pulses is based on nonthermal ablation [46] and may be preferred to minimize the heat-affected zone (HAZ) [46, 47] and maximize the spatial resolution of the machining process [48]. In the case of ns-laser pulses, the HAZ is limited by working at low fluence ($F < 1 \text{ J cm}^{-2}$) [49], and should be as near as possible to its threshold value (F_{th}). In this case, depending on the value of F and the corresponding temperature gradient in the thin film, it has been observed that ablation of the material may proceed mainly through two routes: i) detachment of thin films because of the thermoelastic force (lower F), and ii) ejection of the material after reaching the melting or evaporation temperature (higher F) [43, 49].

In comparison with gaseous environments, only a very few studies report the ablation of a metallic thin film in water. PLA of metal targets in liquid environments is mainly used for synthesizing colloidal dispersion of NPs of highly variable materials [28, 50, 51]. In this framework, ablation of metallic thin films in water has a particular control on both the chemical nature and the size of the produced nanomaterials [52, 53].

The liquid environment is responsible for plasma confinement, which affords higher ablation efficiencies and lower values of F_{th} in comparison to PLA in gas or vacuum [54, 55]. Moreover, the presence of water as an external thermal bath attenuates the problems associated with the HAZ and possible thermal damage, which are not considered to be critical issues as in gaseous environments [38, 56].

In this study, we investigated the value of F_{th} in a water environment for silver (Ag) thin films with a thickness of approximately 50 nm using ns-laser pulses at the wavelength of 532 nm. A self-assembled monolayer (SAM) of (3-mercaptopropyl) trimethoxysilane (MPTS) was used as a chemical adhesion layer for stabilizing the SiO_2/Ag interface in water [57]. The efficiency of material removal was evaluated via optical microscopy, depending on the value of F and number of laser pulses. This implies that thermoelastic force with delamination and phase transformation of the thin films may be responsible for the ablation process. The results are finally applied for demonstrating the regeneration of glass microfluidic reactors dedicated to the continuous-flow synthesis of citrate-stabilized AgNPs, demonstrating that thermoelastic ablation at moderate laser-pulse fluence and repetition rates along with low scanning velocities, can be used in this specific case to obtain cleaning



performances similar to or better than those obtained through the traditional acid treatments in terms of efficiency and time required to completely remove the nanomaterials from the devices used for the synthesis.

2. Materials and methods

2.1. Materials

The Ag pellets used for thin-film deposition were purchased from Kurt J. Lesker Company (U.S.A), with purity >99%. Ethanol, 3-mercaptopropyltrimethoxysilane (MPTS), acetone, and trichloroethylene were purchased from Sigma-Aldrich. Ultrapure deionized water was purchased from a Milli-Q purification system, by Millipore (U.S.A). Silver nitrate (AgNO_3 ; >99.9% pure), sodium borohydride (NaBH_4 ; >99% pure), $\text{Na}_3\text{Citrate}$ (99.9% pure) were acquired from Sigma-Aldrich and used as received. All solutions were prepared using ultrapure water (resistivity of $18.2 \text{ M}\Omega \text{ cm}^{-1}$).

2.2. Synthesis and characterization of citrate-stabilized AgNPs

Citrate-stabilized colloidal AgNPs solutions were synthesized using a glass chip microreactor of $6 \mu\text{l}$ internal volume (Micronit) (figures 1(a), (b)), and two syringe pumps (Future Chemistry) as described in previous works [58, 59]. Solutions of AgNO_3 ($10^{-2} \text{ mol L}^{-1}$) and $\text{Na}_3\text{Citrate}$ ($10^{-2} \text{ mol L}^{-1}$) were prepared by dissolving the salts in ultrapure water. A reducing agent solution of NaBH_4 ($10^{-2} \text{ mol L}^{-1}$) was prepared to promote the chemical reduction of silver ions to AgNPs. The microdevice had two inlet tubes for reagent injection and one output tube for collecting the synthesized material, as shown in figure 1(b). Under continuous flow, AgNO_3 and organic-ligand solutions were introduced into the microreactor at the same flow rate of 0.25 ml min^{-1} . Through the outlet channel, the complex Ag^+ -ligand was dropped directly into the flask containing 10-mL NaBH_4 ($10^{-3} \text{ mol L}^{-1}$) under vigorous magnetic stirring at room temperature (22°C). After 20 min the corresponding AgNPs were stored in the refrigerator for further characterization. The dimensions of the NPs were measured using a field-emission scanning electron microscope (FEG-SEM) (JEOL, JSM-6701F) operating in transmission mode (STEM).

Figure 1(c) depicts a STEM image of the synthesized AgNPs obtained via transmission electron microscopy. Consistent with the results published in [60], the AgNPs have a *log-normal* distribution [50], with an average diameter of approximately 6.7 nm. We verified that even after three cycles of NPs synthesis because of the

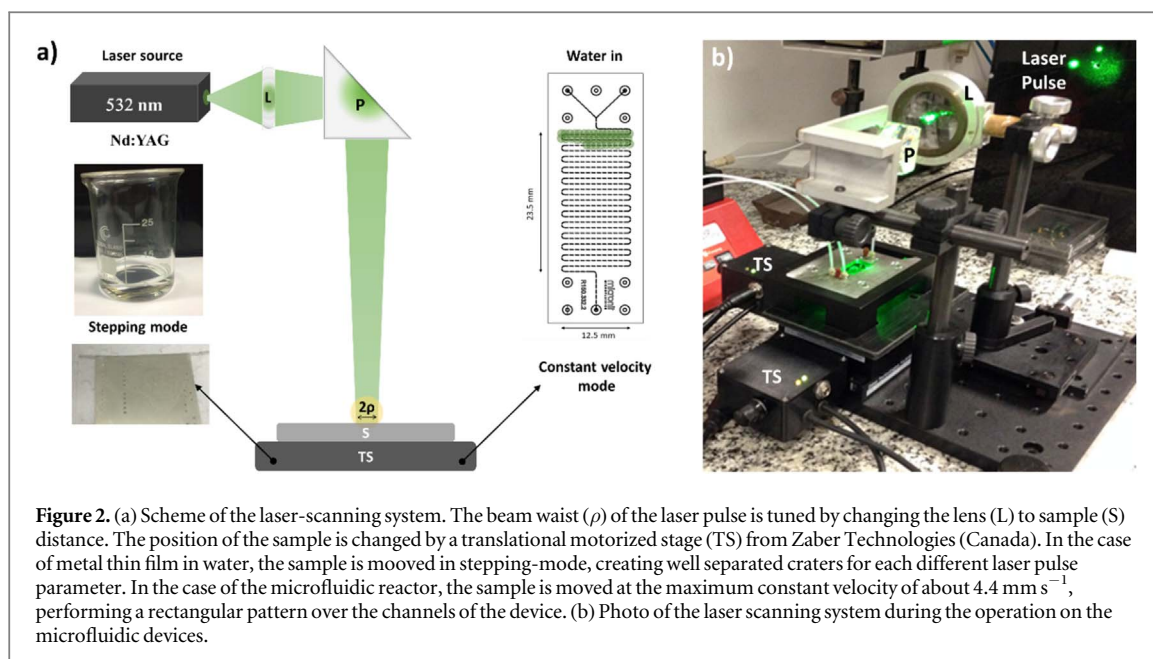


Figure 2. (a) Scheme of the laser-scanning system. The beam waist (ρ) of the laser pulse is tuned by changing the lens (L) to sample (S) distance. The position of the sample is changed by a translational motorized stage (TS) from Zaber Technologies (Canada). In the case of metal thin film in water, the sample is moved in stepping-mode, creating well separated craters for each different laser pulse parameter. In the case of the microfluidic reactor, the sample is moved at the maximum constant velocity of about 4.4 mm s^{-1} , performing a rectangular pattern over the channels of the device. (b) Photo of the laser scanning system during the operation on the microfluidic devices.

deposition of the nanomaterial onto the internal channel's wall and slow clogging of the microchannel, the reproducibility of the optical properties of the nanomaterial was compromised. This is evident in the extinction band of the colloidal dispersion of AgNPs, where the spectral position of the maximum of the localized surface plasmon resonance (LSPR) shifts from 391 nm (fresh microreactor) to a value of approximately 404 nm after five consecutive cycles, indicating a progressive enhancement of the average dimension of the NPs. To retrieve the LSPR band centered at 391 nm (figure 1(d)), the microreactors should be cleaned using the following procedure: (i) flux 5 ml of water (0.25 ml min^{-1}) to eliminate the residual organic ligand; (ii) flux 5 ml of 5% of HNO_3 in water (0.1 ml min^{-1}) to dissolve the NPs; and (iii) flux 5 ml of water (0.25 ml min^{-1}) for eliminating the residual acid. The total time required for the cleaning procedure was approximately 1.5 h.

2.3. Fabrication of the Ag thin films

Before the deposition of the thin film and salinization, BK7 glass substrates were treated using 10-min ultrasonic baths in trichloroethylene, acetone, ethanol, and deionized water. The glasses were dried and placed into a plasma cleaner for hydroxyl group activation before the deposition of the SAM of MPTS, similarly as reported in [57].

The Ag thin films were deposited on the MPTS-treated substrates using an electron beam deposition system model Univex 450, at a pressure of approximately 3×10^{-6} Torr and a deposition rate of approximately 0.5 \AA s^{-1} . The final thin-film thickness of approximately 50 nm was measured via SPR spectroscopy [61, 62].

2.4. Scanning PLA system

For the ablation we used an Nd:YAG pulsed laser source model *Ultra 20*, from Quantel (U.S.A). The pulses had a nominal temporal length of approximately 10 ns, and the repetition rate can be switched from 1 to 50 Hz. Because the laser source emitted pulses simultaneously at both 1064 and 532 nm, we inserted a dichroic mirror with an efficiency $>90\%$ (EKSM Optics, Lithuania) at the output of the laser source to transmit the pulses at the second harmonic frequency. The energy E of the pulses was measured by a pyroelectric detector from ThorLabs (model ES220C, U.S.A.).

As depicted in figure 2(a), the laser pulse at a wavelength of 532 nm was directed toward a prism and deviated perpendicularly onto a lens (L) with a focal length of 13 mm. The focused laser pulse interacted with the sample S (metal thin film or aged microfluidic cell), which is scanned along the horizontal plane by two motorized micrometer translation stages from Zaber Technologies (Canada), operating in single steps or constant scanning velocity modes. In the case of the metal thin film we used the single-step mode, whereas for the ablation of the microfluidic device we used the maximum constant scanning velocity of approximately 4.4 mm s^{-1} . In the latter case, the mechanical base was moved along a rectangular pattern of the same dimensions as the microfluidic device ($23.5 \text{ mm} \times 12.5 \text{ mm}$) and the ablation is performed at a water fluxing rate of about 0.15 ml min^{-1} , starting from the position relative to the entry of the liquid and finishing on the water flow output. The water flux was maintained in a continuous-flow regime using a Future Chemistry (Netherlands) pump system.

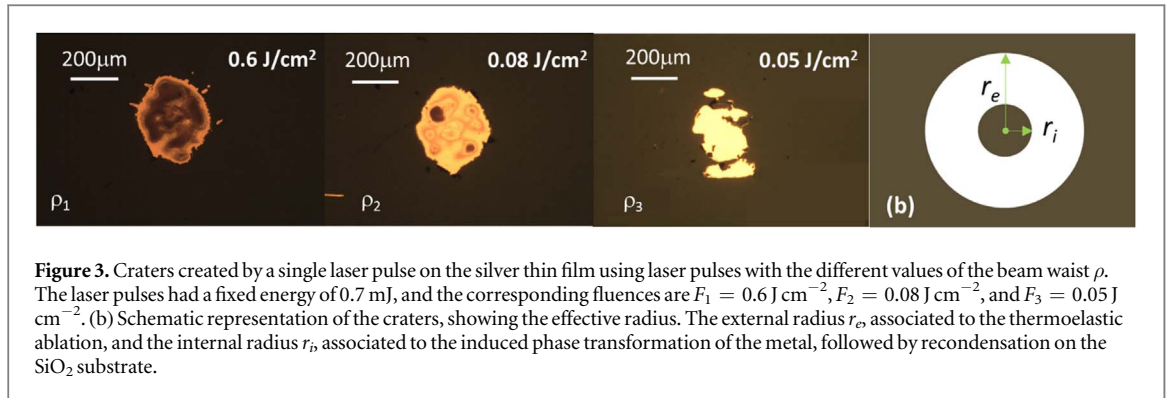


Figure 3. Craters created by a single laser pulse on the silver thin film using laser pulses with the different values of the beam waist ρ . The laser pulses had a fixed energy of 0.7 mJ, and the corresponding fluences are $F_1 = 0.6 \text{ J cm}^{-2}$, $F_2 = 0.08 \text{ J cm}^{-2}$, and $F_3 = 0.05 \text{ J cm}^{-2}$. (b) Schematic representation of the craters, showing the effective radius. The external radius r_e , associated to the thermoelastic ablation, and the internal radius r_i , associated to the induced phase transformation of the metal, followed by recondensation on the SiO_2 substrate.

2.5. Measurement of the threshold and working fluence

In the approximation of a Gaussian spatial profile of the E-field of the laser pulse, the working fluence F of the laser pulse is defined as $F = \frac{E}{\pi/2 \rho^2}$, where E is the total energy of the pulse and ρ is the beam waist on the surface of the target, i.e., the radial distance at which the energy (or the intensity, or the same fluence F) decreases by a factor $1/e^2$ in comparison to the axial value [63]. F and ρ were controlled by varying the lens to the sample distance represented in figure 2, and their value was evaluated by the comparative method described in detail in the supporting information of our previous research [64]. In this method, the PLA of the Ag thin film was conducted using three conditions for the beam waist on the target: $\rho_1 = 270 \mu\text{m}$, $\rho_2 = 710 \mu\text{m}$, and $\rho_3 = 910 \mu\text{m}$ with an error of approximately 15%. For each value of the beam waist on the target, the resulting craters were investigated via optical microscopy (Motic, model BA210, U.S.A) depending on both the number of laser pulses and the energy E of the pulse. When using a single pulse, the dependence of the effective radius r_{eff} of the crater in function of E can be used to measure the threshold fluence F_{th} for the ablation of the Ag thin films according to the well-known relation given as follows:

$$\ln F = \frac{2}{\rho^2} r_{\text{eff}}^2 + \ln F_{th}, \quad (1)$$

which gives the value of F_{th} via linear interpolation of the experimental data [39, 65].

Based on the experimental results, the concept of an effective radius r_{eff} is particularly useful when the crater formed has an irregular shape. In this case the effective radius is determined by calculating the total effective area A_{eff} of the crater using the *ImageJ* free software and applying the simple relation: $r_{\text{eff}}^2 = A_{\text{eff}} / \pi$.

3. Experimental results and discussion

3.1. Analysis of craters created by PLA on Ag thin film

The craters created by PLA of the Ag thin films by a single-laser pulse with the three beam waists are represented in figure 3. The energy of the laser pulse was fixed at 0.8 mJ so that the three cases correspond to working fluences $F_1 = 0.6 \text{ J cm}^{-2}$, $F_2 = 0.08 \text{ J cm}^{-2}$, and $F_3 = 0.05 \text{ J cm}^{-2}$. Notably, the fluences were measured using the aforementioned procedure with an error of approximately 30%. The optical images were obtained in transmission mode so that dark regions are associated with the presence of the metal.

These images give important information about the origin of the PLA process depending on the working fluence. As explained in [43, 49], depending on the working fluence, the increase in temperature at the metal/substrate interface after absorption of the laser pulse may cause different phenomena. As depicted in figure 4, when the temperature is below the fusion point, a thermoelastic force is induced by PLA, which locally enhances the mechanical stress of the thin film. If the thermoelastic force exceeds the adhesion force at the $\text{SiO}_2/\text{MPTS}/\text{Ag}$ interface, the thin film is ablated by delamination. At higher values of F , the temperature at the interface can rapidly increase and provoke phase transformation (melting and vaporization) of the thin film, with ejection of the material as liquid drops or ionized metal clusters, eventually recombining in water as AgNPs [66], or recondensing on the glass surface in disordered structures [38].

In figure 3, using a fluence $F_3 = 0.05 \text{ J cm}^{-2}$, no metal residuals were observed in the ablated region. Vice versa, when F is of the order of 0.1 J cm^{-2} , traces of Ag are clearly visible in the central portion of the crater. This is because the laser-pulse energy distribution, ideally modeled as a Gaussian, is not uniform, and decreases from the center to the border of the laser spot. Hence, while the peripheral regions of the craters still exhibit thermoelastic-induced delamination, the central portions start to provoke phase transformation of the material. While a part of this material is definitively ejected, the remaining material recondenses on the glass surface in irregular structures. As previously reported by K L Choo *et al* [38], this interesting phenomenon can be

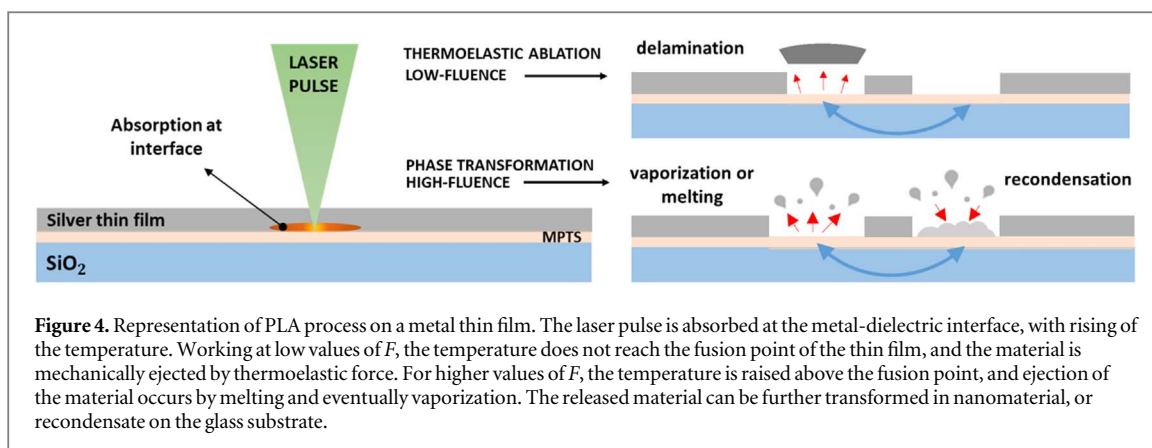


Figure 4. Representation of PLA process on a metal thin film. The laser pulse is absorbed at the metal-dielectric interface, with rising of the temperature. Working at low values of F , the temperature does not reach the fusion point of the thin film, and the material is mechanically ejected by thermoelastic force. For higher values of F , the temperature is raised above the fusion point, and ejection of the material occurs by melting and eventually vaporization. The released material can be further transformed in nanomaterial, or recondensate on the glass substrate.

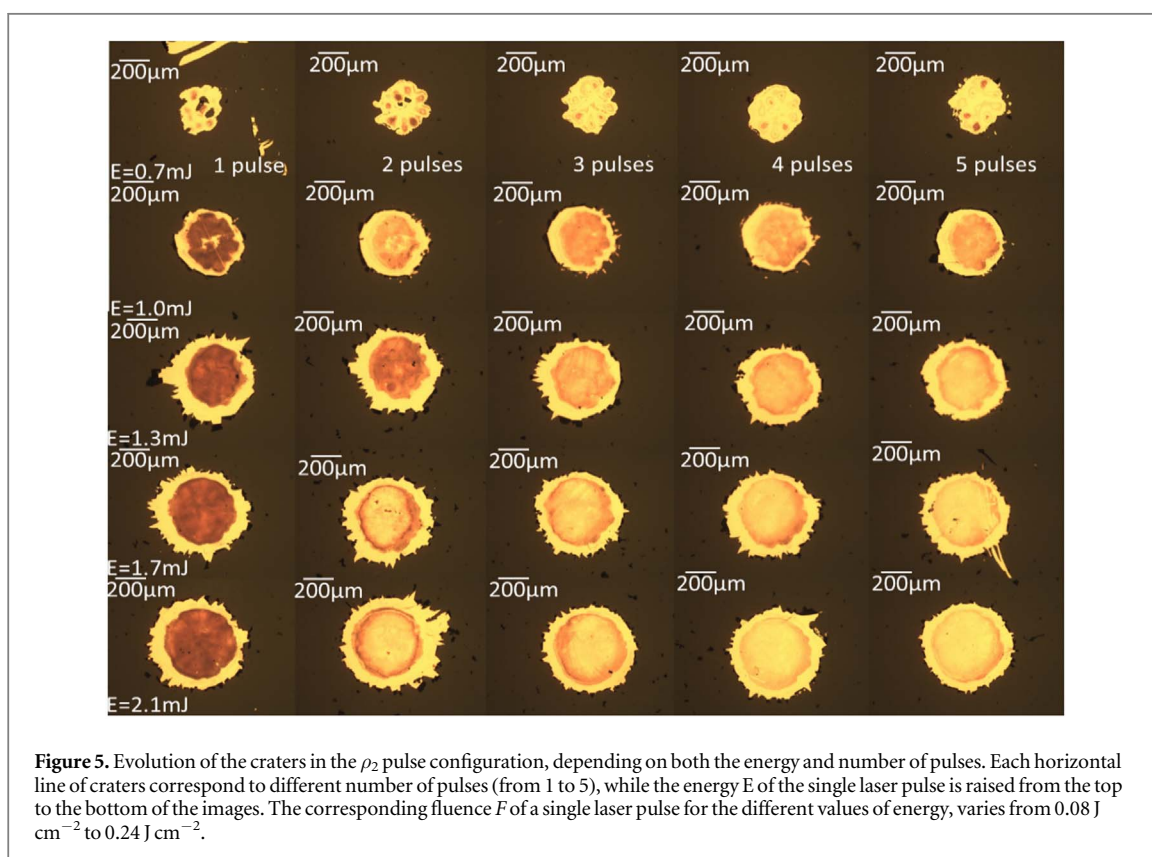


Figure 5. Evolution of the craters in the ρ_2 pulse configuration, depending on both the energy and number of pulses. Each horizontal line of craters correspond to different number of pulses (from 1 to 5), while the energy E of the single laser pulse is raised from the top to the bottom of the images. The corresponding fluence F of a single laser pulse for the different values of energy, varies from 0.08 J cm^{-2} to 0.24 J cm^{-2} .

attributed to the presence of water as an external environment, which confines the plasma in the proximity of the thin film and reduces its lifetime owing to rapid decrease in the temperature [66]. Owing to the overlap of delamination, phase transformation, and recondensation of the material in the case of PLA of thin metal films in water, it is convenient to define two characteristic radii of the craters, as represented in figure 3(b). Herein, we define an external radius r_e , corresponding to the maximum distance at which we observe delamination and an internal radius r_i , corresponding to the maximum distance at which recondensation is observed.

The evolution of the craters in the ρ_2 pulse configuration is shown in figure 5, where the energy and number of pulses were different. The corresponding fluence of a single-laser pulse for the different values of energy varies from 0.08 to 0.24 J cm^{-2} .

Considering the single-pulse craters, when F is increased, both the internal and external radii (r_i , r_e) become bigger, consistent with equation (1). Increasing the number of pulses causes progressive removal of the recondensed material, thus the best experimental results were obtained for the lowest and highest fluences. Generally, we observed that with multiple pulses, the metal residuals were not definitively removed from the ablated regions with the same efficiency as the single-pulse pure thermoelastic ablation.

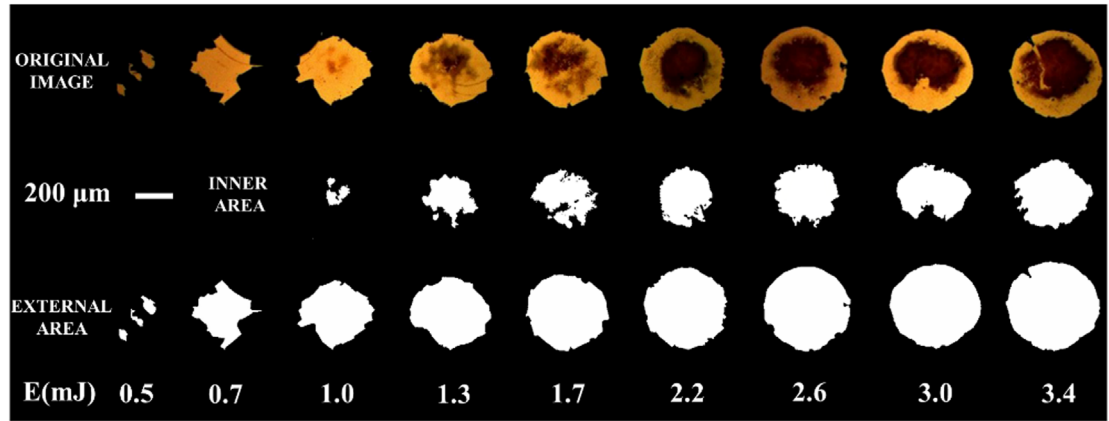


Figure 6. On the upper and bottom parts of the figure are represented the optical images of the craters in the ρ_3 pulse configuration before and after the software elaboration, respectively. A single pulse was used to form the craters, with energy increasing from the left to the right direction of the image. The corresponding fluence F of a single laser pulse for the different values of energy, varies from 0.04 J cm^{-2} to 0.26 J cm^{-2} .

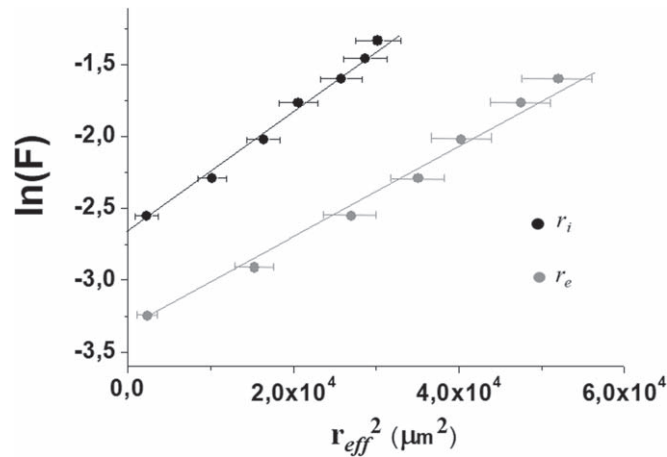


Figure 7. Dependence of $\ln(F)$ on the square of the effective radius r_{eff}^2 in the ρ_3 configuration. In both cases two set of data were traced, corresponding to the internal (r_i , black points) and external (r_e , grey points) effective radius. The errors bars are associated to the repetition of the experiments on three silver thin films with the same thickness of about 50 nm. The continuous lines represent the linear fit on the experimental data, by the use of equation (1).

To more accurately evaluate the threshold fluence F_{TE} associated with the thermoelastic force (TE), different craters were created by single-laser pulses in the defocused configuration ρ_3 . The optical images of the craters are depicted in figure 6, where the working fluence was varied from from 0.04 to 0.26 J cm^{-2} .

Moreover, for lower values of F , only the thermoelastic ablation process occurs; however, with increasing the fluence, the metal undergoes phase transformation and recondensation on the glass substrate. These craters were used to calculate the effective internal and external radii. The images of the craters after the software elaboration are reported at the bottom of each pristine optical image.

With this procedure, the values of $\ln F$ were plotted in function of r_{eff}^2 . The corresponding graph is shown in figure 7. In the graph, the two lines are related to the effective radius r_e and r_i , associated with the threshold fluences F_{TE} and F_{PT} , respectively. The errors bars in the graph were calculated considering three ablated samples.

From the linear fit of the experimental data, we obtain $F_{TE} = 37 \text{ mJ cm}^{-2}$ and $F_{PT} = 70 \text{ mJ cm}^{-2}$. S Reich *et al* [67] measured $F_{th} = 5 \text{ mJ cm}^{-2}$ for Ag, by inspection of the craters generated by PLA in water with single-laser pulses with a ns duration. Considering the ablation of Ag thin films in water, very few studies report results on the measurement of F_{th} , do not consider the use of an organic layer between the metal and the glass and do not investigate the thermoelastic regime. P A Danilov *et al* [68, 69] recently measured values between 0.1 and 0.4 J cm^{-2} on films with a thickness of 50 nm, depending on both temporal duration and dimension of the laser pulse. Considering experiments using ns-laser pulse, L Huang *et al* [49] observed that a clear ablation pattern could still

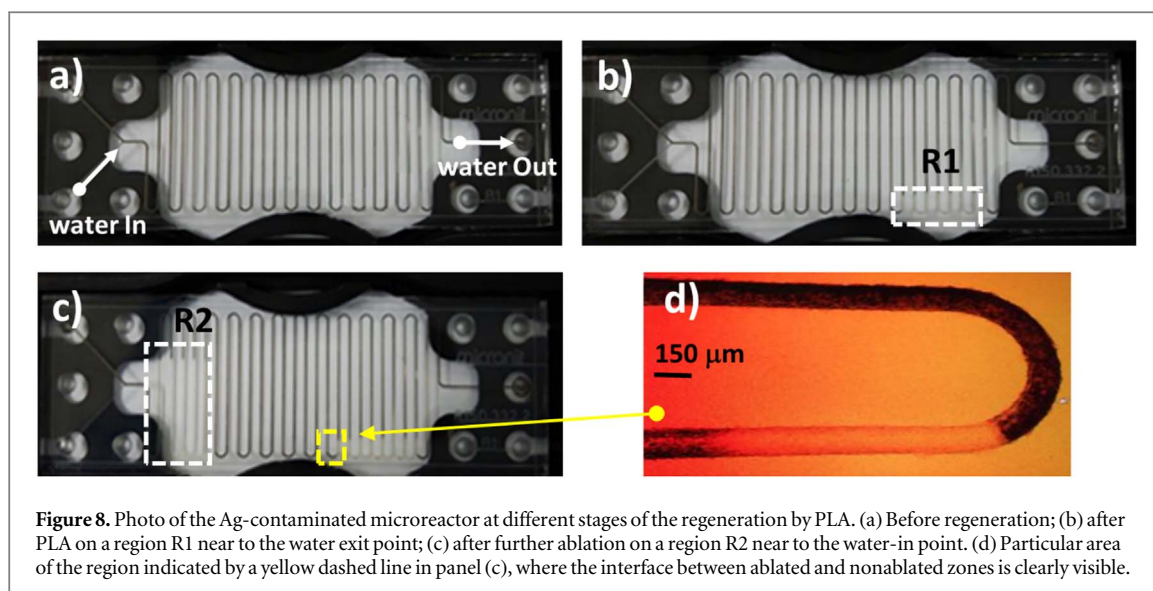


Figure 8. Photo of the Ag-contaminated microreactor at different stages of the regeneration by PLA. (a) Before regeneration; (b) after PLA on a region R1 near to the water exit point; (c) after further ablation on a region R2 near to the water-in point. (d) Particular area of the region indicated by a yellow dashed line in panel (c), where the interface between ablated and nonablated zones is clearly visible.

be formed for a working fluence of 0.1 J cm^{-2} so that F_{th} is lower than this value considering their investigation. Our results are consistent with the literature although none of the cited works refer to a possible thermoelastic effect because the working fluences were too high to observe a pure thermoelastic ablation.

3.2. Regeneration of microfluidic reactors by thermoelastic PLA in water

Citrate-stabilized AgNPs were synthesized using the microfluidic reactor, following the aforementioned procedure. The microreactor was used consecutively for five iterations of the synthesis process, after which the surface of the microfluidic channels was covered by a coating of metallic Ag, as shown in figure 8(a).

Under these conditions, water was injected through the microfluidic channels and simultaneously a region R1 of the device near the water output position was ablated using the proposed laser-scanning system in the ρ_3 pulse configuration to ensure the experimental condition necessary for thermoelastic ablation. After that, a region R2 near to the water-in contact was ablated under the same experimental conditions. As shown in figures 8(b) and (c), from the optical inspection, no differences are observed between regions R1 and R2; thus, we infer that for the regeneration of the reactors by scanning thermoelastic ablation, it is not necessary to start from the water-in point. Figure 8(d) shows an expanded view of the region R1 in figure 8(b) where the border between ablated and nonablated regions of the device is clearly visible.

The complete regeneration of the chemical device was performed at the maximum scanning velocity of approximately 4.4 mm s^{-1} and a laser-pulse repetition rate of 10 Hz. Because $\rho_3 = 1020 \mu\text{m}$, each region of the microreactor was interacting with an average of five laser pulses. The total time required for the complete regeneration was of approximately 200 s. The reason for this result is that the scanning system has a constant velocity along the longest side of the microreactor (23.5 mm) and scans the shorter side (12.5 mm) at single steps of $400 \mu\text{m}$. Figure 9 shows the optical images of the channels of microreactors subject to different treatments.

From the optical analysis, we infer that the efficiency of the material removal from the microchannels is similar when it is performed by PLA and acid treatment. After both treatments we verified that, unlike before the removal, the experimental fluxing rate of water was equal to the nominal rate controlled by the continuous-flow pump, indicating that the channels were ready to be used for further synthesis cycles. Under these conditions, as it was expected, the AgNPs obtained after the synthesis recovered the original LSPR position centered around 391 nm (figure 1(d)). Although our experimental results show that complete regeneration of the microfluidic device can be realized within few minutes using low-fluence pulses at moderate scanning velocities, the use of laser equipment with a repetition rate on the order of kHz and scanning systems with velocities up to m s^{-1} [43] would allow completion of the removal process within few seconds. The proposed sustainable regeneration of microfluidic reactors may be not economically viable for research groups without the disposability of a proper laser source, but it is definitely relevant for the scientific community working in fabrication of glass based microfluidic devices by PLA, and their further application to different chemical processes.

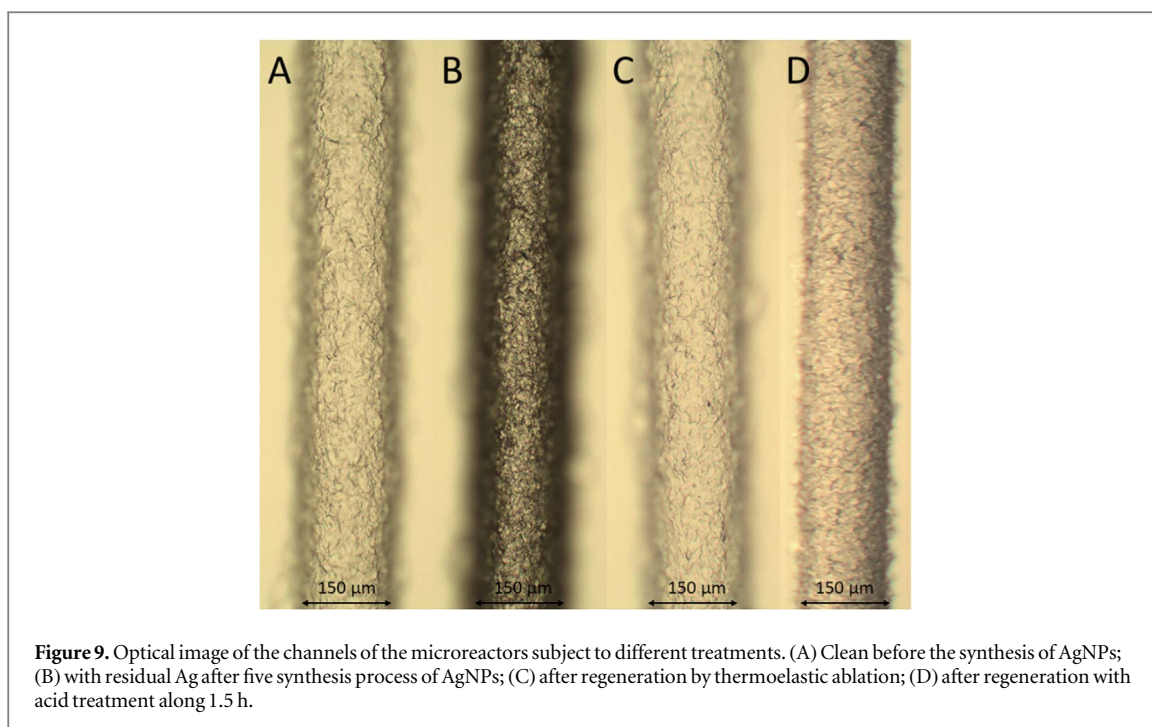


Figure 9. Optical image of the channels of the microreactors subject to different treatments. (A) Clean before the synthesis of AgNPs; (B) with residual Ag after five synthesis process of AgNPs; (C) after regeneration by thermoelastic ablation; (D) after regeneration with acid treatment along 1.5 h.

4. Conclusions

We investigated the ablation process of a Ag thin film in a water environment deposited over SiO_2 substrate with MPTS organic adhesion layer, observing different physical processes allowing the removal of the material, with distinct threshold fluences. Thermoelastic ablation was responsible for the delamination of the thin film when the fluence approximately exceeded 40 mJ cm^{-2} and phase transformation of the thin film and subsequent condensation on the SiO_2 surface was observed for a fluence approximately exceeding 70 mJ cm^{-2} . Although several pulses were needed to complete the removal of material after phase transformation, thermoelastic ablation was effective at the single-pulse level. This peculiar characteristic was used to demonstrate the possibility of using an easily affordable experimental configuration, with low-fluence and moderate scanning velocity, to apply PLA as a green technique for the regeneration of clogged glass microreactors used for the synthesis of citrate-stabilized AgNPs. The results demonstrate that PLA can indeed be used in this particular experimental configuration for the regeneration of the glass microdevices, with performances equal to or better than the classic acid treatments in terms of material removal and operation time. From this successful proof of concept, future research will be devoted to investigating the wider applicability of the technique using different substrates (PMMA and PDMS), 3D geometries, and different types of material clogging the devices.

Acknowledgments

This study was financed in part by the Coordenação de Aperfeiçoamento de Pessoal de Nível Superior - Brasil (CAPES) - Finance Code 001. Funding from FAPERJ for processes E-26/010.100622/2018, E-26/010.001646/2019, E-26/010.002138/2019 and E-26/010.000980/2019 are acknowledged. We acknowledge also CNPq and the Instituto Nacional de Engenharia de Superfícies (INCT-INES) (Processes 423349/2018-0 and 465423/2014-0).

Data availability statement

The data that support the findings of this study are available upon reasonable request from the authors.

ORCID iDs

Omar Ginoble Pandoli  <https://orcid.org/0000-0002-2220-7817>

Tommaso Del Rosso  <https://orcid.org/0000-0002-0600-4139>

References

- [1] Elvira K S, Solvas X C I, Wootton R C R and Demello A J 2013 The past, present and potential for microfluidic reactor technology in chemical synthesis *Nat. Chem.* **5** 905–15
- [2] West J, Becker M, Tombrink S and Manz A 2008 Micro total analysis systems: latest achievements *Anal. Chem.* **vol. 80** 4403–19
- [3] Temiz Y, Lovchik R D, Kaigala G V and Delamarche E 2015 Lab-on-a-chip devices: how to close and plug the lab? *Microelectron. Eng.* **132** 156–75
- [4] Chan H N *et al* 2016 Simple, cost-effective 3D printed microfluidic components for disposable, point-of-care colorimetric analysis *ACS Sens.* **1** 227–34
- [5] Ren K, Zhou J and Wu H 2013 Materials for microfluidic chip fabrication *Acc. Chem. Res.* **46** 2396–406
- [6] Tian Z, Ge X, Wang Y and Xu J 2018 *Nanoparticles and Nanocomposites with Microfluidic Technology* (Elsevier Inc)
- [7] Wyss H M, Blair D L, Morris J F, Stone H A and Weitz D A 2006 Mechanism for clogging of microchannels *Physical Review E - Statistical, Nonlinear, and Soft Matter Physics* **74** 1–4
- [8] Dressaire E and Sauret A 2017 Clogging of microfluidic systems *Soft Matter* **13** 37–48
- [9] Luo G, Du L, Wang Y, Lu Y and Xu J 2011 Controllable preparation of particles with microfluidics *Particuology* **9** 545–58
- [10] Mashaghi S, Abbaspourrad A, Weitz D A and van Oijen A M 2016 Droplet microfluidics: a tool for biology, chemistry and nanotechnology *TrAC - Trends Anal. Chem.* **82** 118–25
- [11] Kaminski T S and Garstecki P 2017 Controlled droplet microfluidic systems for multistep chemical and biological assays *Chem. Soc. Rev.* **46** 6210–26
- [12] Duraiswamy S and Khan S A 2009 Droplet-based microfluidic synthesis of anisotropic metal nanocrystals *Small* **5** 2828–34
- [13] Khan S A, Günther A, Schmidt M A and Jensen K F 2004 Microfluidic synthesis of colloidal silica *Langmuir* **20** 8604–11
- [14] Takagi M, Maki T, Miyahara M and Mae K 2004 Production of titania nanoparticles by using a new microreactor assembled with same axle dual pipe *Chem. Eng. J.* **101** 269–76
- [15] Utada A S, Fernandez-Nieves A, Stone H A and Weitz D A 2007 Dripping to jetting transitions in coflowing liquid streams *Phys. Rev. Lett.* **99** 1–4
- [16] Yaghmur A, Ghazal A, Ghazal R, Dimaki M and Svendsen W E 2019 A hydrodynamic flow focusing microfluidic device for the continuous production of hexosomes based on docosahexaenoic acid monoglyceride *Phys. Chem. Chem. Phys.* **21** 13005–13
- [17] Shin D, Kim Y and Moon H S Fate and toxicity of spilled chemicals in groundwater and soil environment: I. Strong acids *Environ. Health Toxicol.* **33** e2018019
- [18] Sreedhar I, Singh M and Raghavan K V 2013 Scientific advances in sulfuric acid free toluene nitration *Catal. Sci. Technol.* **3** 2499–508
- [19] Kim I T, Sinha T K, Lee J, Lee Y and Oh J S 2021 Ultrasonic treatment: an acid-free green approach toward preparing high-performance activated carbon from lignin *Ind. Eng. Chem. Res.* **60** 2439–46
- [20] Kumar H *et al* 2021 Efficient green protocols for the preparation of pyrazolopyrimidines *ChemistrySelect* **6** 5807–37
- [21] Inman G, Prodius D and Nlebedim I C 2021 Recent advances in acid-free dissolution and separation of rare earth elements from the magnet waste *Clean Technol. Recycl.* **1** 112–23
- [22] Willmott P R and Huber J R 2000 Pulsed laser vaporization and deposition *Rev. Mod. Phys.* **72** 315–28
- [23] Liu X, Du D and Mourou G 1997 Laser ablation and micromachining with ultrashort laser pulses *IEEE J. Quantum Electron.* **33** 1706–16
- [24] Hibst R and Keller U 1989 Experimental studies of the application of the Er:YAG laser on dental hard substances: I. Measurement of the ablation rate *Lasers Surg. Med.* **9** 338–44
- [25] Chung S H and Mazur E 2009 Surgical applications of femtosecond lasers *J. Biophotonics* **2** 557–72
- [26] Chakravarthi M, Shilpakar R and Shankar K 2009 Carbon dioxide laser guidelines *J. Cutan. Aesthet. Surg.* **2** 72–9
- [27] Siano S *et al* 2012 Laser cleaning in conservation of stone, metal, and painted artifacts: state of the art and new insights on the use of the Nd:YAG lasers *Appl. Phys. A Mater. Sci. Process.* **106** 419–46
- [28] Amendola V and Meneghetti M 2013 What controls the composition and the structure of nanomaterials generated by laser ablation in liquid solution? *Phys. Chem. Chem. Phys.* **15** 3027–46
- [29] Cheung J and Horwitz J 1992 Pulsed laser deposition history and laser-target interactions *MRS Bull.* **17** 30–6
- [30] Wlodarczyk K L, Hand D P and Maroto-Valer M M 2019 Maskless, rapid manufacturing of glass microfluidic devices using a picosecond pulsed laser *Sci Rep.* **9** 1–13
- [31] Sugioka K *et al* 2014 Femtosecond laser 3D micromachining: a powerful tool for the fabrication of microfluidic, optofluidic, and electrofluidic devices based on glass *Lab Chip* **14** 3447–58
- [32] Liu C *et al* 2012 Fabrication of three-dimensional microfluidic channels inside glass using nanosecond laser direct writing *Opt. Express* **20** 4291
- [33] Wlodarczyk K L *et al* 2018 Rapid laser manufacturing of microfluidic devices from glass substrates *Micromachines* **9** 1–14
- [34] Butkutė A and Jonušauskas L 2021 3D manufacturing of glass microstructures using femtosecond laser *Micromachines* **12** 499
- [35] Hossain M R and Konari P R 2021 Laser micromachining of glass substrates for microfluidics devices *AIP Conf. Proc.* **2324**, 060002
- [36] Roth G-L, Esen C and Hellmann R 2017 Femtosecond laser direct generation of 3D-microfluidic channels inside bulk PMMA *Opt. Express* **25** 18442
- [37] Isiksacan Z, Guler M T, Aydogdu B, Bilican I and Elbuken C 2016 Rapid fabrication of microfluidic PDMS devices from reusable PDMS molds using laser ablation *J. Micromechanics Microengineering* **26** 35008
- [38] Choo K L, Ogawa Y, Kanbargi G, Otra V, Raff L M and Komanduri R 2004 Micromachining of silicon by short-pulse laser ablation in air and under water *Mater. Sci. Eng. A* **372** 145–62
- [39] Sikora A, Grojo D and Sentis M 2017 Wavelength scaling of silicon laser ablation in picosecond regime *J. Appl. Phys.* **122** 045702
- [40] Jaeggi B, Neuenschwander B, Schmid M, Murali M, Zuercher J and Hunziker U 2011 Influence of the pulse duration in the ps-regime on the ablation efficiency of metals *Phys. Procedia* **12** 164–71
- [41] Semerok A *et al* 1999 Experimental investigations of laser ablation efficiency of pure metals with femto, pico and nanosecond pulses *Appl. Surf. Sci.* **138–139** 311–4
- [42] Hashida M, Semerok A F, Gobert O, Petite G, Izawa Y and Wagner J F 2002 Ablation threshold dependence on pulse duration for copper *Appl. Surf. Sci.* **197–198** 862–7
- [43] Bovatsek J, Tamhankar A, Patel R S, Bulgakova N M and Bonse J 2010 Thin film removal mechanisms in ns-laser processing of photovoltaic materials *Thin Solid Films* **518** 2897–904
- [44] Heo J, Min H and Lee M 2015 Laser micromachining of permalloy for fine metal mask *Int. J. Precis. Eng. Manuf. - Green Technol.* **2** 225–30
- [45] Compaan A D, Matulionis I and Nakade S 2000 Laser scribing of polycrystalline thin films *Opt. Lasers Eng.* **34** 15–45

- [46] Kim B *et al* 2021 Selective laser ablation of metal thin films using ultrashort pulses *Int. J. Precis. Eng. Manuf. - Green Technol.* **8** 771–82
- [47] Amer M S, El-Ashry M A, Dosser L R, Hix K E, Maguire J F and Irwin B 2005 Femtosecond versus nanosecond laser machining: Comparison of induced stresses and structural changes in silicon wafers *Appl. Surf. Sci.* **242** 162–7
- [48] Hermann J *et al* 2006 Selective ablation of thin films with short and ultrashort laser pulses *Appl. Surf. Sci.* **252** 4814–8
- [49] Jing Huang L, Ming Zhang G, Li H, Jia Li B, Ying Wang Y and Fei Ren N 2020 Selective laser ablation and patterning on Ag thin films with width and depth control *J. Mater. Sci., Mater. Electron.* **31** 4943–55
- [50] Del Rosso T *et al* 2018 Biocompatible Au@Carbyonoid/Pluronic-F127 nanocomposites synthesized by pulsed laser ablation assisted CO₂ recycling *Appl. Surf. Sci.* **441** 347–55
- [51] Del Rosso T *et al* 2016 Synthesis of oxocarbon-encapsulated gold nanoparticles with blue-shifted localized surface plasmon resonance by pulsed laser ablation in water with CO₂ absorbers *Nanotechnology* **27** 1–11
- [52] Scaramuzza S, Zerbetto M and Amendola V 2016 Synthesis of gold nanoparticles in liquid environment by laser ablation with geometrically confined configurations: insights to improve size control and productivity *J. Phys. Chem. C* **120** 9453–63
- [53] Nikov R G, Nedyalkov N N, Nikov R G and Karashanova D B 2018 Nanosecond laser ablation of Ag–Au films in water for fabrication of nanostructures with tunable optical properties *Appl. Phys. A Mater. Sci. Process.* **124** 1–9
- [54] Krstulović N, Shannon S, Stefanuik R and Fanara C 2013 Underwater-laser drilling of aluminum *Int. J. Adv. Manuf. Technol.* **69** 1765–73
- [55] Mahdiah M H, Nikbakht M, Eghlimi Moghadam Z and Sobhani M 2010 Crater geometry characterization of Al targets irradiated by single pulse and pulse trains of Nd:YAG laser in ambient air and water *Appl. Surf. Sci.* **256** 1778–83
- [56] Prakash S, Acherjee B, Kuar A S and Mitra S 2013 An experimental investigation on Nd:YAG laser microchanneling on polymethyl methacrylate submerged in water *Proc. Inst. Mech. Eng. Part B J. Eng. Manuf.* **227** 508–19
- [57] Del Rosso T, Zaman Q, Cremona M, Pandoli O and Barreto A R J 2018 SPR sensors for monitoring the degradation processes of Eu(dbm) 3 (phen) and Alq 3 thin films under atmospheric and UVA exposure *Appl. Surf. Sci.* **442** 759–66
- [58] Ginoble Pandoli O *et al* 2019 A regioselective coating onto microarray channels of bamboo with chitosan-based silver nanoparticles *J. Coatings Technol. Res.* **16** 999–1011
- [59] Pandoli O *et al* 2016 Colloidal silver nanoparticles: an effective nano-filler material to prevent fungal proliferation in bamboo *RSC Adv.* **6** 98325–36
- [60] Farooq S *et al* 2018 Engineering a plasmonic sensing platform for *Candida albicans* antigen identification *J. Nanophotonics* **12** 1
- [61] Del Rosso T, Sánchez J E H, Carvalho R D S, Pandoli O and Cremona M 2014 Accurate and simultaneous measurement of thickness and refractive index of thermally evaporated thin organic films by surface plasmon resonance spectroscopy *Opt. Express* **22** 18914
- [62] Del Rosso T *et al* 2017 Enhanced stability of plasmonic metal thin films by CVD grown graphene transfer *Thin Solid Films* **644** 65–70
- [63] Born M *et al* 1999 *Principles of Optics* 7th ed. (Cambridge: Cambridge University Press) no. March0521642221
- [64] Fulvio D, Fuks Maron L, Cires Perez Y, Tahir and Del Rosso T 2021 Micrometeorite bombardment simulated by ns-pulsed laser ablation: morphological characterization of the impact craters *Icarus* **366** 114532
- [65] Liu J M 1982 Simple technique for measurements of pulsed Gaussian-beam spot sizes *Opt. Lett.* **7** 196
- [66] Amendola V and Meneghetti M 2009 Laser ablation synthesis in solution and size manipulation of noble metal nanoparticles *Phys. Chem. Chem. Phys.* **11** 3805–21
- [67] Reich S *et al* 2017 Fluence threshold behaviour on ablation and bubble formation in pulsed laser ablation in liquids *ChemPhysChem* **18** 1084–90
- [68] Danilov P A *et al* 2020 Femtosecond laser ablation of thin silver films in air and water under tight focusing *Opt. Mater. Express* **10** 2717
- [69] Smirnov N A *et al* 2020 Femtosecond laser ablation of a thin silver film in air and water *Opt. Quantum Electron.* **52** 1–8